Richtmyer-Meshkov instability in liquid metal flows: influence of cavitation and magnetic fields

Roman Samulyak *, Yarema Prykarpatskyy

Center for Data Intensive Computing,
Brookhaven National Laboratory, Upton, NY 11973

Abstract

The influence of magnetic fields and cavitation on the Richtmyer - Meshkov type instability in liquid mercury have been studied numerically. Numerical results shed light on the evolution of the proposed Muon Collider target which will be designed as a pulsed jet of mercury interacting with high intensity proton beams in a strong magnetic field. We have shown that a uniform magnetic field significantly reduces amplitudes and velocities of surface instabilities and is able to stabilize the jet during period of time typical for the jet breakup at zero magnetic field. We have developed a simple homogeneous two-phase equation of state for modeling the evolution of waves in mercury in the presence of cavitation bubbles and studied the Richtmyer-Meshkov instability in the presence of cavitation.

Key words: Richtmyer-Meshkov instability, MHD, Cavitation
PACS: 47.50.Ma, 47.55.Bx, 47.65.+a

1 Introduction

Studies of the shock-induced Richtmyer-Meshkov (RM) instability is important from both fundamental and applied points of view. RM instability arises when an interface between two different fluids or gases (ie.: different densities) is rapidly accelerated. RM instability can be considered as a special case of the Rayleigh-Taylor instability which occurs when a density interface experiences a constant acceleration. The instability manifests itself in the form of

* Corresponding author.
Email addresses: rosamu@bnl.gov (Roman Samulyak), yarpry@bnl.gov (Yarema Prykarpatskyy).

the unbounded growth of initial perturbations on the interface [2,4,11]. RM instability is important in both natural phenomena (supernovae) and technological applications (inertial confinement fusion) [5]. More generally, it is typical for processes involving explosions.

In this paper, we present results of the numerical study of RM instability in the presence of cavitation and magnetic fields. Namely, we have studied the growth of surface instabilities in conducting liquid jets in strong magnetic fields due to external energy depositions. Our study was motivated by the target problem for the proposed Muon Collider. The target will be designed as a pulsed jet of mercury (high Z-liquid) interacting with a high energy proton beam in the presence of a strong magnetic field [20]. Interactions of strong shocks or shock type waves with the surface of a free moving liquid mercury jet may create major complications in the target operation. Previous numerical [10,21] and experimental [6,7,15] studies of the mercury jet - proton beam interaction in the absence of a magnetic field indicate that the mercury jet will be completely broken into a system of droplets due to the proton energy deposition within several milliseconds. This makes it impossible to deposit multiple proton pulses in the mercury jet and creates implications for the target design. We have studied the Richtmyer-Meshkov type instability in the mercury target including MHD effects and showed that magnetic field significantly reduces surface instabilities.

The system of free surface MHD equations is an example of a coupled hyperbolic - elliptic (or parabolic) system in a geometrically complex and dynamically evolving domain. We have developed a numerical method for solving such systems and the corresponding parallel software. The numerical methods for the hyperbolic subsystem is based on FronTier, a hydrodynamics code with free interface support [9]. FronTier uses front tracking [8], a numerical technique for solving systems of conservation laws in which the evolution of discontinuities is determined through solutions of the associated Riemann problem. The elliptic or parabolic subsystem of the MHD equations is solved using an embedded boundary finite volume discretization method in the domain bounded by the free interface [13]. However, in the present geometry of our 2D numerical experiments the solution of the elliptic problem can be obtain analytically. This allows us to skip the expensive step of solving the elliptic problem numerically. This simplification is not valid for other configurations of the jet and for 3D problems in particular.

Numerical simulations performed with a single phase equation of state (EOS) for liquid mercury (stiffened polytropic EOS) have shown that the strength of rarefaction waves in the mercury target significantly exceeds the mercury cavitation threshold [24]. We believe that the formation of cavities takes place in strong rarefaction waves and cavitation bubbles influence the wave dynamics in mercury and the Richtmyer-Meshkov instability of the jet surface. Exper-

imental results tend to confirm this assumption. Therefore the modeling of cavitation and liquid properties under extreme thermodynamic conditions is essential for obtaining accurate predictions based on numerical simulations. We have developed a simple homogeneous two-phase equation of state for modeling wave dynamics in fluids in the presence of cavitation bubbles. We have applied this model to study the interaction of mercury with an intensive proton pulse in the geometry typical for Muon Collider/Neutrino Factory experiments at the Brookhaven National Laboratory (BNL) and CERN. In this paper, we discuss simulation results and the future work on the cavitation modeling.

The paper is organized as follows. In Section 2, we formulate the main system of MHD equations and discuss some simplifying assumptions. The numerical implementation of the MHD system in the FronTier code is given in Section 3. In Section 4, we present results of the numerical simulations of the Richtmyer-Meshkov instability in free surface MHD jets and discuss applications to the Muon Collider target design. Section 5 contains the description of the two-phase EOS model. Results of the numerical simulation of mercury thimble experiments are discussed in Section 6. Finally, we conclude the paper with a summary of our results and perspectives for future work.

2 Equations for Magnetohydrodynamics of Free Surface Liquids

The system of MHD equations [12,16] contains a hyperbolic system of the mass, momentum and energy conservation equations for the fluid and a parabolic equation for the evolution of the magnetic field:

$$\frac{\partial \rho}{\partial t} = -\nabla \cdot (\rho \mathbf{u}), \tag{1}$$

$$\rho \left(\frac{\partial}{\partial t} + \mathbf{u} \cdot \nabla \right) \mathbf{u} = -\nabla P + \rho \mathbf{g} + \frac{1}{c}(\mathbf{J} \times \mathbf{B}), \tag{2}$$

$$\rho \left(\frac{\partial}{\partial t} + \mathbf{u} \cdot \nabla \right) E = -P \nabla \cdot \mathbf{u} + \rho \mathbf{u} \cdot \mathbf{g} + \frac{1}{\sigma}\mathbf{J}^2, \tag{3}$$

$$\frac{\partial \mathbf{B}}{\partial t} = \nabla \times (\mathbf{u} \times \mathbf{B}) - \nabla \times (\frac{c^2}{4\pi\sigma} \nabla \times \mathbf{B}), \tag{4}$$

$$\nabla \cdot \mathbf{B} = 0. \tag{5}$$

Here $\mathbf{u}$, ρ and E are the velocity, density, and the specific internal energy of the fluid, respectively, P is the pressure, $\mathbf{g}$ is the gravitational acceleration, $\mathbf{B}$ is the magnetic field induction, $\mathbf{J} = \nabla \times \mathbf{H}$ is the current density distribution, and σ is the fluid conductivity. The magnetic field $\mathbf{H}$ and magnetic induction

$\mathbf{B}$ are related by the magnetic permeability coefficient μ: $\mathbf{B} = \mu\mathbf{H}$. In the system (1) - (5), we neglected effects of the heat conduction and viscosity.

The system (1-3) must be closed with an equation of state (EOS). We are especially interested in fluid behavior under extreme thermodynamic conditions. EOS models are discussed in Section 5.

The following boundary conditions must be satisfied at the free fluid interface:

i) the normal component of the velocity field is continuous across the material interface.

ii) the normal and tangential components of the magnetic field at the material interface are related as

$$\mathbf{n} \cdot (\mathbf{B}_2 - \mathbf{B}_1) = 0, \tag{6}$$

$$\mathbf{n} \times (\mathbf{H}_2 - \mathbf{H}_1) = \frac{4\pi}{c}\mathbf{K}, \tag{7}$$

where $\mathbf{K}$ is the surface current density. Note that $\mathbf{K} = 0$ for mercury.

The behavior of a fluid in the presence of electromagnetic fields is governed to a large extent by the magnitude of the conductivity. For fluid at rest (4) reduces to the diffusion equation

$$\frac{\partial \mathbf{B}}{\partial t} = \frac{c^2}{4\pi\mu\sigma}\Delta\mathbf{B}. \tag{8}$$

This means that an initial configuration of magnetic field will decay with typical diffusion time

$$\tau = \frac{4\pi\mu\sigma L^2}{c^2},$$

where L is a characteristic length of the spatial variation of $\mathbf{B}$. Despite being good enough conductors, most of liquid metals including mercury are characterized by small diffusion times (33 microseconds for a mercury droplet of 1 cm radius) compared to some solid conductors (1 s for a copper sphere of 1 cm radius). Therefore the magnetic field penetration in such liquid conductors can be considered as an instantaneous process. This allows us to assume that the magnetic field is constant in time (low magnetic Reynolds number approximation, see [18]), and to obtain the current density distribution using Ohm's law

$$\mathbf{J} = \sigma\left(-\mathrm{grad}\phi + \frac{1}{c}\mathbf{u} \times \mathbf{B}\right), \tag{9}$$

where ϕ is the electric field potential. The potential ϕ satisfies the following Poisson equation

$$\Delta\phi = \frac{1}{c}\mathrm{div}(\mathbf{u}\times\mathbf{B}), \tag{10}$$

and the Neumann boundary conditions

$$\left.\frac{\partial\phi}{\partial\mathbf{n}}\right|_{\Gamma} = \frac{1}{c}(\mathbf{u}\times\mathbf{B})\cdot\mathbf{n}, \tag{11}$$

where $\mathbf{n}$ is a normal vector at the fluid free surface Γ. This approach is applicable for the study of MHD processes in mercury typical for Muon Collider applications. Notice that the assumption of a constant in time magnetic field also excludes Alfven waves, which do not have a major impact on the wave dynamics and surface evolution in our problems.

The linear stability analysis of thin conducting liquid jets moving along the axis of a uniform magnetic field [1] and the corresponding analysis for the mercury jet used in the Muon Collider [10] show that an axial uniform field tends to stabilize the jet surface against the natural Rayleigh instability. In this paper, we show that magnetic fields also stabilizes the Richtmyer-Meshkov instability induced by an external energy deposition.

3 Numerical Implementation

In this section, we will describe numerical ideas implemented in the FronTier MHD code. The system of MHD equations used in our studies (1) - (3), (10) - (11) is a coupled hyperbolic - elliptic system in geometrically complex moving domain. We have developed a numerical method for solving such systems and the corresponding parallel software. The numerical method treats the MHD system in the operator splitting manner. We use the front tracking hydro code FronTier with free interface support for solving the hyperbolic subsystem (1) - (3). The Poisson equation (10) - (11) is solved using an embedded boundary method for elliptic equations in irregular domains.

FronTier represents interfaces as lower dimensional meshes moving through a volume filling grid [8]. The traditional volume filling finite difference grid supports smooth solutions located in the region between interfaces. The location of the discontinuity and the jump in the solution variables are defined on the lower dimensional grid or interface. The dynamics of the interface comes from the mathematical theory of Riemann solutions, which are an idealized solutions of single jump discontinuities for a conservation law. FronTier is capable

of tracking three dimensional interfaces and resolving their topological changes [9]. Notice that since we are primarily interested in the contact discontinuity propagation, we restrict ourselves to the Riemann problem for a hydro system of equations and therefore neglect some elementary waves typical for the MHD Riemann problem. Some features of the FronTier hyperbolic solvers include the use of high resolution methods such as MUSCL with a large selection of Riemann solvers and realistic models for the equation of state.

The existence of a tracked surface, across which physical parameters and the solution change discontinuously, has important implications for the solution of an elliptic or parabolic system. In a forthcoming paper, we will describe an approached based on the finite volume discretization which uses the embedded boundary method for irregular cells near the interface. In the current problem geometry, however, the elliptic equation (10) - (11) has a trivial solution which allows us to skip the expensive step of solving the elliptic problem numerically. Namely, in the case of a 2D jet moving along the axis of a uniform magnetic field $\mathrm{div}(\mathbf{u}\times\mathbf{B}) = 0$ and $(\mathbf{u}\times\mathbf{B})\cdot\mathbf{n} = 0$, where $\mathbf{n}$ is a normal vector at the fluid free surface. This implies $\phi = \text{const}$ and $\mathbf{J} = \frac{\sigma}{c}\mathbf{u}\times\mathbf{B}$. This simplification is not valid for other configurations of the jet and for 3D problems in particular.

4 Numerical Simulation of the Richtmyer-Meshkov Instability in Liquid Jets

In this section, we present results of the numerical simulation of the Richtmyer-Meshkov type instability in liquid metal (mercury) jets in magnetic fields due to the proton energy deposition. The problem was inspired by the muon collider target application. The target [20] is shown schematically in Figure 1. It will contain a series of mercury jet pulses of about 0.5 cm in radius and 60 cm in length. Each pulse will be shot at a velocity of 30-35 m/sec into a 20 Tesla magnetic field at a small angle (0.1 rad) to the axis of the field. When the jet reaches the center of the magnet, it is hit with a 3 ns proton pulse depositing about 100 J/g of energy in the mercury.

In the numerical simulation, the initial mercury jet is taken as a 15 cm long and 1 cm diameter ideal cylinder with no surface perturbations. The influence of the proton pulse was modeled by adding the proton beam energy density to the internal energy density of mercury at a single time step. The distribution of the proton energy deposition in mercury was approximated by a 2D. The liquid was modeled using the stiffened polytropic equation of state [3,17]

$$P = (\gamma_l - 1)\rho(E + E_\infty) - \gamma_l P_\infty$$

with the adiabatic exponent $\gamma_l = 3.2$ and the stiffening constant $P_\infty =$

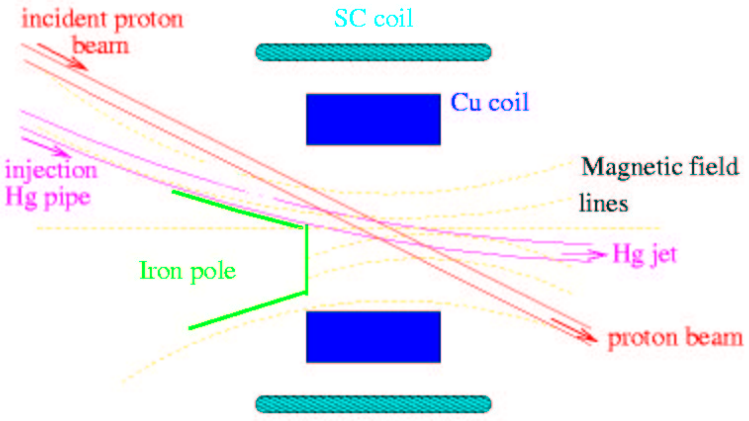

Fig. 1. Schematic of the muon collider target.

$8 \cdot 10^{10} g/(cm \cdot sec^2)$. The polytropic gamma law gas [3] was used for the ambient gas. Numerical simulations on a 2100 X 700 grid were performed on 32 processors of a distributed memory cluster of Pentium processors running RedHat Linux. The evolution of the mercury jet due to a single proton pulse energy deposition is depicted in Figure 2.

The external energy deposition in the mercury jet resulted in an instantaneous heating and formation of a high pressure domain and strong waves. A multiple reflection of pressure waves from the wall caused a series of surface perturbations which evolved in the form of narrow radial jets. The first pressure wave initialized small grid related surface perturbations. During the later time evolution, neighboring radial jets merged forming a spatial distribution of RM type surface instabilities independent of the grid size. Due to the interaction of the perturbed interface with the next reflected pressure wave, a period doubling of the surface instabilities was observed during a short period of time. This period doubling was diminished as radial jets merged during the instability growth. Notice that a shock (pressure) wave reflects from the mercury – gas interface as a rarefaction wave and the result of the rarefaction wave reflection is a shock (pressure) wave. Such a multiple reflection of pressure/rarefaction waves from the jet surfaces and a series of RM type instabilities on the jet surface resulted from the use of the stiffened polytropic equation of state capable of modeling a single phase fluid with tension.

Figure 3 depicts results of the numerical simulation of the Richtmyer - Meshkov type instability evolution in the presence of a strong magnetic field. A uniform magnetic field was applied to the mercury jet along the axis. The Lorentz force due to induced currents reduced both the wave speed in the liquid and the velocity of surface instabilities. As a result, surface instabilities were suppressed in a 10 Tesla magnetic field during times typical for the jet breakup at zero magnetic field. The velocity reduction of jet surface instabilities in the magnetic field is showed in Figure 4.

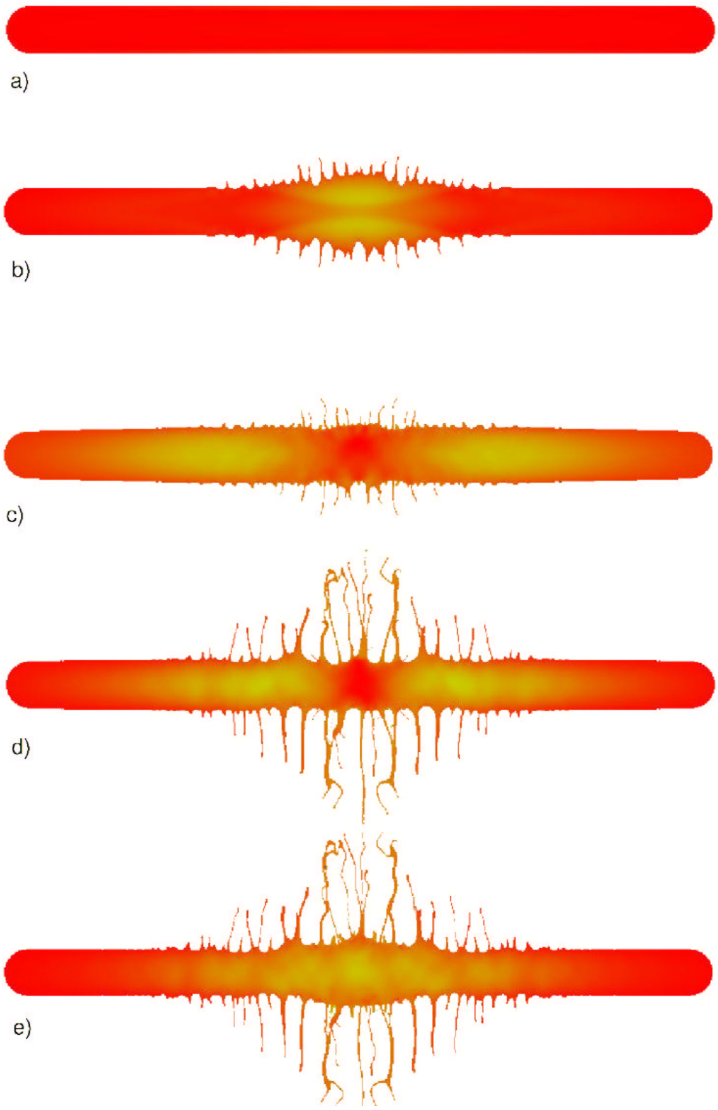

Fig. 2. Evolution of the mercury jet due to the proton energy deposition, B = 0: a) Initial shape of the jet, t = 0; b) Surface instabilities due to the second reflected pressure wave, t = 40 μs; c) Interaction of the third reflected pressure wave with the surface, t = 45 μs; d) Surface instabilities due to the third reflected pressure wave, t = 59 μs; e) Interaction of the fourth reflected pressure wave with the surface, t = 67 μs.

5 Equation of State Model for Two-phase Fluid

Numerical simulation discussed in the previous section showed that domains with large values of liquid tension developed during the jet evolution. The existence of such domains of tension or "negative pressure" in rarefaction waves is a typical feature of the stiffened polytropic EOS, which is a single phase EOS model for liquids. The absolute values of the "negative pressure" in our

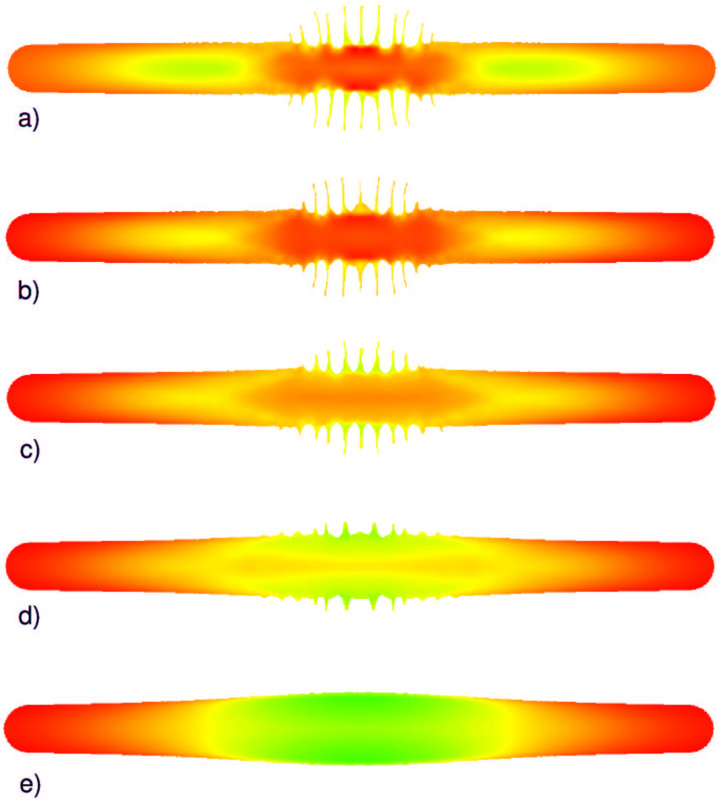

Fig. 3. Stabilizing of the mercury jet by the longitudinal magnetic field: a) B = 0, b) B = 2T, c) B = 4T, d) B = 6T, e) B = 10T.

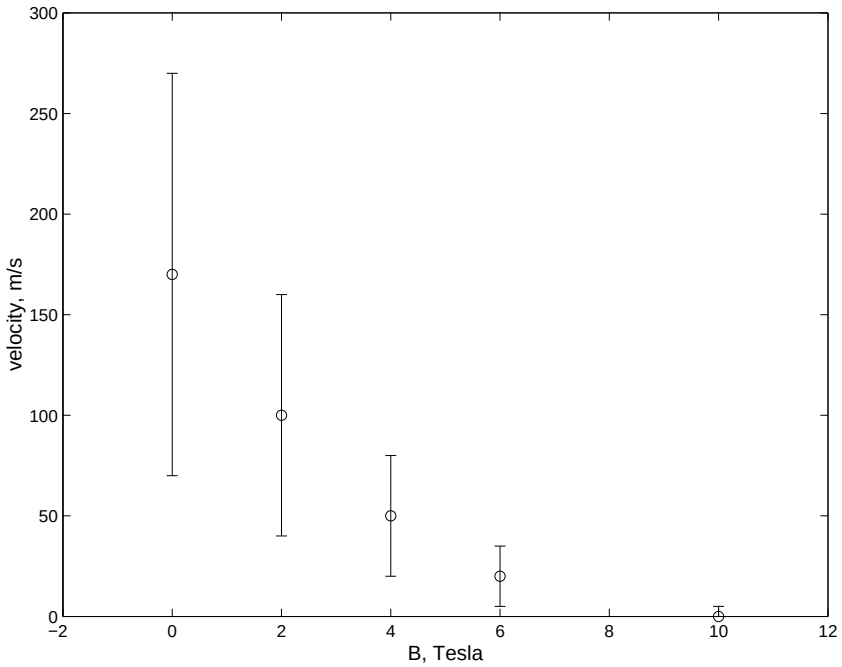

Fig. 4. Velocity of jet surface instabilities in the magnetic field.

simulations significantly exceeded the critical value of the mercury cavitation threshold estimated in [24]. Therefore we believe that the formation of cavities takes place in strong rarefaction waves and cavitation bubbles influence the wave dynamics in mercury and the Richtmyer-Meshkov instability of the jet surface. Analysis of experimental results tend to confirm this assumption. Therefore the modeling of cavitation and liquid properties under extreme thermodynamic conditions is essential for obtaining accurate predictions based on numerical simulations. In this section, we will derive an equilibrium homogeneous model for a two-phase system in the isentropic approximation. The application of this EOS to the Muon Collider/Neutrino Factory experiments will be described in Section 6.

The isentropic approximation is valid for numerous physically important phenomena characterized by small time scales. The homogeneous flow approximation provides the simplest technique for analyzing two-phase (or multiple phase) flows. Suitable average properties are determined and the mixture is treated as a pseudofluid that obeys the usual equation of single-component flow. The isentropic approximation reduces by one the number on independent variables defining the thermodynamic state. As a result, all thermodynamic states in our EOS will be functions of only density. The proposed EOS consists of three branches. The pure vapor and liquid branches are described by the polytropic and stiffened polytropic EOS models reduced to a single isentrope. The two branches are connected by a model for the liquid-vapor mixture. The analytical expressions for thermodynamic functions in all branches as well and their connection are described below.

5.1 Liquid phase model

The equation of the stiffened polytropic EOS model describing the pure liquid phase is

$$P = (\gamma_l - 1)\rho(E + E_\infty) - \gamma_l P_\infty, \tag{12}$$

where γ_l is the adiabatic exponent for the liquid, and P_∞ and E_∞ are two model parameters defining the maximum tension (the maximum value of the "negative pressure" achievable in the liquid) and the energy shift constant correspondingly. E_∞ can be used to obtain the quantitative agreement of the internal energy of the liquid at normal conditions with experimental data. The expression for the entropy is

$$S = \frac{R_l}{\gamma_l - 1}(\log(P + P_\infty) - \gamma_l \log\rho), \tag{13}$$

where R_l is a model constant similar to the universal gas constant $R = 8.314$ erg/degrees.

Reducing the equation (12) to an isentrope $S = S_0$ and using the main thermodynamic identity,

$$dE = -PdV + TdS,$$

the following expressions can be derived:

$$P = \eta_l \rho^{\gamma_l} - P_\infty, \tag{14}$$

$$E = \frac{\eta_l}{\gamma_l - 1}\rho^{\gamma_l - 1} + \frac{P_\infty}{\rho} - E_\infty, \tag{15}$$

$$a_l^2 = \gamma_l \eta_l \rho^{\gamma_l - 1}, \tag{16}$$

$$T = \frac{\eta_l}{R_l}\rho^{\gamma_l - 1}, \tag{17}$$

where

$$\eta_l = \exp\left(\frac{S_0(\gamma_l - 1)}{R_l}\right), \tag{18}$$

and a_l is the speed of sound in liquid.

5.2 A model for the liquid - vapor mixture

The following expression for the speed of sound in an equilibrium homogeneous mixture of liquid and gas has been derived and experimentally validated [22,23]

$$\frac{1}{a^2} = (\alpha\rho_{sat,v} + (1-\alpha)\rho_{sat,l})\left(\frac{\alpha}{\rho_{sat,v}{a_{sat,v}}^2} + \frac{1-\alpha}{\rho_{sat,l}{a_{sat,l}}^2}\right), \tag{19}$$

where $\rho_{sat,v}$, $\rho_{sat,l}$, $a_{sat,v}$, $a_{sat,l}$ are the density and the speed of sound of vapor and liquid in saturation points, respectively, and α is the void fraction

$$\alpha = \frac{\rho - \rho_{sat,l}}{\rho_{sat,v} - \rho_{sat,l}}.$$

Integrating the sound speed with respect to the density, the following pressure - density relation along an isentrope can be obtained [22]

$$P = P_{sat,l} + P_{vl}\log\left[\frac{\rho_{sat,v}{a_{sat,v}}^2(\rho_{sat,l} + \alpha(\rho_{sat,v} - \rho_{sat,l}))}{\rho_{sat,l}(\rho_{sat,v}{a_{sat,v}}^2 - \alpha(\rho_{sat,v}{a_{sat,v}}^2 - \rho_{sat,l}{a_{sat,l}}^2))}\right], \tag{20}$$

where $P_{sat,l}$ is the liquid pressure in the saturation point and

$$P_{vl} = \frac{\rho_{sat,v} {a_{sat,v}}^2 \rho_{sat,l} {a_{sat,l}}^2 (\rho_{sat,v} - \rho_{sat,l})}{\rho_{sat,v}{}^2 {a_{sat,v}}^2 - \rho_{sat,l}{}^2 {a_{sat,l}}^2}. \tag{21}$$

Using the second law of thermodynamic at constant entropy and the expressions above, we can derive an analytical expression for the specific internal energy of the vapor-liquid mixture. The formula is omitted here for the sake of simplicity.

5.3 Vapor phase model

The equation of the polytropic EOS model describing the pure vapor phase is

$$P = (\gamma_v - 1) E \rho, \tag{22}$$

where γ_v is the adiabatic exponent of the vapor. The expression for the entropy is

$$S = \frac{R}{\gamma_v - 1} (\log(P - \gamma_v \log\rho). \tag{23}$$

Similar to the pure liquid case, we can perform the isentropic reduction and obtain

$$P = \eta_v \rho^{\gamma_v}, \tag{24}$$
$$E = \frac{\eta_v}{\gamma_v - 1} \rho^{\gamma_v - 1}, \tag{25}$$
$$a_v^2 = \gamma_v \eta_v \rho^{\gamma_v - 1}, \tag{26}$$
$$T = \frac{\eta_v}{R} \rho^{\gamma_v - 1}, \tag{27}$$

where

$$\eta_v = \exp\left(\frac{S_0(\gamma_v - 1)}{R}\right), \tag{28}$$

and a_v is the speed of sound in vapor.

We will describe a procedure for defining all coefficients in the formulas (12)-(31) using a minimal set of input parameters. The resulting EOS satisfies the

smoothness and stability requirements [17]. We choose the following minimal set of input parameters most of which are measurable quantities:

$$
\begin{aligned}
&\rho_{sat,l}, && \text{density of the saturated liquid}\\
&\rho_{sat,v}, && \text{density of the saturated vapor}\\
&P_{sat,l}, && \text{pressure of the saturated liquid}\\
&T_{sat,l}, && \text{temperature of the saturated liquid}\\
&C_V, && \text{specific heat at constant volume of the liquid}\\
&a_{sat,l}, && \text{sound speed of the saturated liquid}\\
&a_{sat,v}, && \text{sound speed of the saturated vapor}\\
&\text{or} &&\\
&\gamma_v, && \text{adiabatic exponent of the saturated vapor.}
\end{aligned}
\tag{29}
$$

Then all parameters of the EOS can be defined uniquely using the following procedure.

1. If $a_{sat,v}$ is given in the input set (29), calculate $P_{sat,v}$ using (20)-(21) and input parameters (29). Then find γ_v from (24) and (26)

$$\gamma_v = a_{sat,v}^2 \frac{\rho_{sat,v}}{P_{sat,v}}.$$

If γ_v is instead given as an input parameter, solve numerically a system of nonlinear equations involving (20)-(21), (24), and (26) for $a_{sat,v}$. Then find $P_{sat,v}$ as above.

2. Find η_v from (24) substituting $\rho = \rho_{sat,v}$.

3. Find $E_{sat,v}$ using (25).

4. Find the change of the specific internal energy ΔE in the mixed phase using the expression for mixed state internal energy.

5. Find $E_{sat,l}$ as

$$E_{sat,l} = E_{sat,v} + \Delta E.$$

6. Find γ_l as

$$\gamma_l = \frac{1}{2} + \sqrt{\frac{1}{4} + \frac{a_{sat,l}^2}{T_{sat,l} C_V}},$$

which is a solution of the quadratic equation arising from definitions

$$T_l = \frac{P_\infty}{R_l \rho_l}, \quad a^2_{sat,l} = \frac{\gamma_l P_\infty}{\rho_l}, \quad C_V = \frac{R_l}{\gamma_l - 1}.$$

Here we used only one solution of the quadratic equation which satisfies the thermodynamic requirement $\gamma_l > 0$ and assumed that $P << P_\infty$. Find R_l and P_∞ using the last expressions for T_l and C_V.

7. Find η_l and E_∞ using (14) and (15) at $\rho = \rho_{sat,v}$.

9. Find $T_{sat,v}$ using (27) and the value of the universal gas constant R.

Note that the calculation of entropy for the liquid and vapor phases using (13) and (23), respectively, may lead to different numerical values of the entropy in both phases for a given choice of input parameters. This, however, does not contradict the isentropic assumption. All simplified models define entropy through the integration of the second law of thermodynamics and, as a result, the entropy always contains an arbitrary additive constant. To define an absolute value of the entropy the 3rd law of thermodynamics is required. The Nernst theorem states that $S = 0$ at zero absolute temperature. All simplified thermodynamic models, however, can not describe the behavior of materials at temperatures close to zero. Since the Nernst theorem can not be satisfied within the polytropic or stiffened polytropic EOS approximations, all three models used in our derivation contain arbitrary additive constants for the entropy which can be (implicitly in our derivation) chosen to satisfy the constant entropy requirement.

6 Numerical Simulation of Mercury Thimble Experiments

To study the influence of proton pulse induced thermal shocks on mercury targets, a series of experiments were conducted at the Alternating Gradient Synchrotron (AGS) at BNL and On-Line Isotope Mass Separator facility (ISOLDE) at CERN [6,7,15]. We will discuss here some experimental and numerical simulation results of the mercury thimble studies.

The schematic of the mercury thimble experiment is shown in Figure 5. The volume of the thimble excavated in a stainless steel bar is 1.3 cm^3. It consists from bottom to top of a half sphere (r = 6 mm), and a vertical cylinder (r = h = 6 mm). The mercury has a free surface in up-direction, where it can expand to. The proton pulse is schematically denoted by the green dashed line. It has approximately Gaussian distribution and the intensity range of $0.6 - 17 \cdot 10^{12}$ protons at energy 24 GeV.

Figure 6, obtained with high speed shadow photography, depicts the mercury splash due to the interaction with a 3.7 teraproton pulse [6,7]. The grid on the images is 1 cm x 1 cm.

We have performed numerical simulations of the mercury splash evolution in the thimble using the FronTier code with the two-phase equation of state

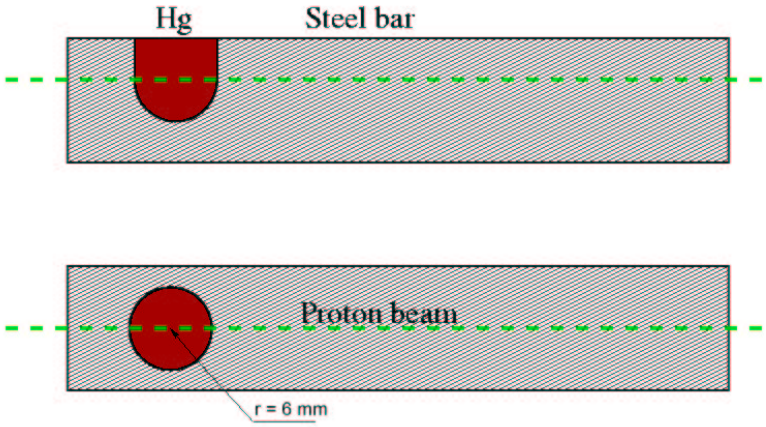

Fig. 5. Schematic of the steel bar with a mercury thimble.

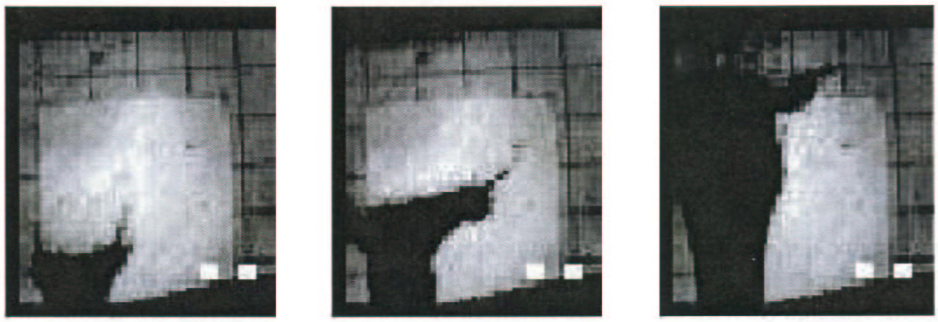

Fig. 6. Images of the mercury splash evolution due to the interaction with a pulse of $3.7 \cdot 10^{12}$ protons at energy 24 GeV. Experiments were performed at BNL AGS.

model described in the previous section. To calculate the actual energy deposition in the mercury due to the interaction with a proton pulse, we used the results of MARS code simulations performed by N. Mokhov [19]. Figure 7 shows an image sequence of the mercury splash evolution in the thimble.

We have studied the evolution of the mercury splash in the thimble at different values of the proton intensity and the r.m.s. spot size of the beam, and compared our results with experimental data.

Figure 8 shows a reasonably good agreement of experimental and computed velocity of the mercury surface as a function of the r.m.s. spot size of the beam. The blue point on the experimental curve corresponding to the BNL AGS experiment is not exact. It was extrapolated from results obtained at much lower beam intensity and contains a large amount of uncertainty. There is no exact knowledge of the energy deposition distribution as well. Therefore, we can conclude that the time scale of the numerically computed mercury splash evolution is in agreement with experimental measurements. We have also reproduced accurately the dependence of the mercury surface velocity on the beam intensity at early times. We would like to emphasize that we were not able to obtain a good quantitative comparison with experiments using the previous one-phase stiffened polytropic EOS model for mercury.

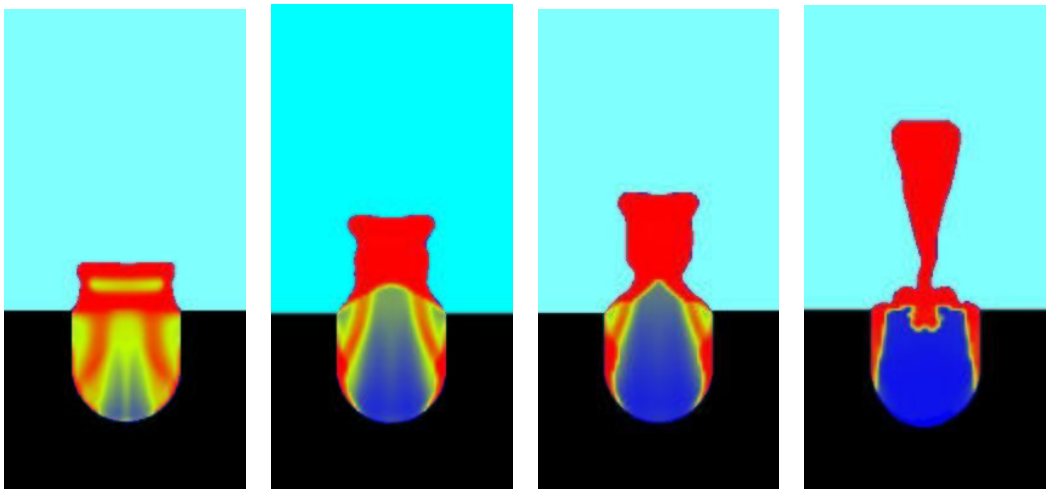

(a) t=0.24 ms (b) t=0.48 ms (c) t=0.61 ms (d) t=1.0 ms

Fig. 7. Numerical simulation of the mercury splash in the thimble

This also confirms the importance of cavitation for the dynamics of waves and the evolution of the Richtmyer-Meshkov instability of the free surface.

However, numerical simulation do not capture some experimentally observable fine effects in the splash evolution such as the reduction of the splash velocity during first 2 microseconds after the arrival of the proton pulse [6]. We believe that this velocity reduction was caused by a reduction of the mercury internal energy due to cavitation. Because of the incomplete thermodynamics of our EOS, the code can not capture such effects without significant improvements of the EOS model. We will describe briefly our current work in this direction in the next section.

7 Conclusions

In this paper, we described a numerical approach based on the method of front tracking for the numerical simulation of magnetohydrodynamic free surface flows and studied the influence of cavitation and magnetic fields on the Richtmyer-Meshkov instability in mercury induced by an external energy deposition. The numerical simulation shed light on the evolution of the proposed Muon Collider target. The target will be designed as a pulsed jet of mercury interacting with strong proton beams in a 20 Tesla magnetic field. Without a magnetic field, the instantaneous heating of mercury and the formation of high pressure region due to the proton energy deposition cause strong waves traveling in the radial direction. Multiple reflections of pressure/rarefaction waves from the mercury jet - ambient gas interface lead to Richtmyer-Meshkov instabilities of the jet surface. The growth of surface instabilities and the breakup of the mercury jet can create difficulties for the

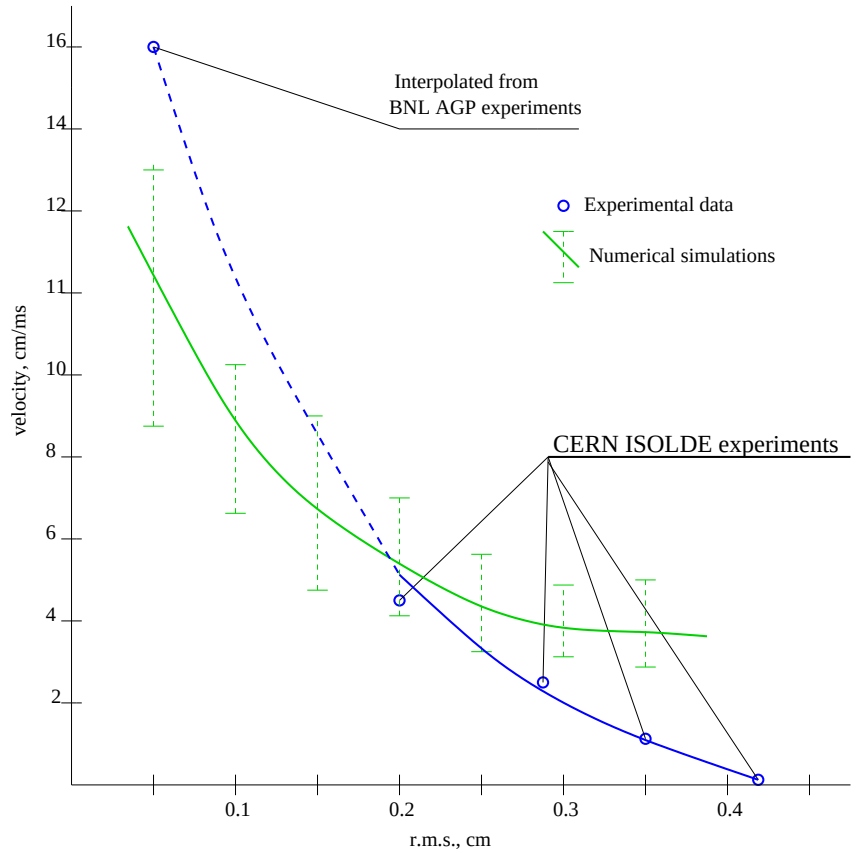

Fig. 8. Velocity of the mercury splash in the thimble as a function of the r.m.s. spot size of the beam.

Muon Collider target design. However, a strong uniform axial magnetic field significantly reduces the amplitude and velocity of RM instabilities as well as the velocity of waves. We have shown that a 10 Tesla magnetic field is able to stabilize the jet during period of times typical for the jet breakup at zero magnetic field. We would like to emphasize strong dependence of the dynamics of shock waves and their interaction with the surface on the nature and parameters of the equation of state and qualitative nature of these results. In current MHD simulations, we used a stiffened polytropic equation of state for mercury. Such an EOS describes a one phase fluid with tension. It was estimated that strong rarefaction waves in the jet lead to the cavitation of mercury and cavitation bubbles influence the dynamics of waves. In order to study this phenomena, we have developed in the isentropic approximation a simple homogeneous EOS with the phase transition (cavitation) support and applied it to the numerical study of the mercury splash evolution typical for BNL and CERN Neutrino Factory experiments. We have obtained a good agreement of the time scale of the numerically computed mercury splash velocity with experimental data for a wide range of proton beam parameters. Some disagreements with experiments of the mercury splash evolution at early times can be explained by the incomplete thermodynamics of our equation of state model. To improve the modeling of the cavitation dynamics, we have

been working on a full thermodynamics equation of state model coupled to a Rayleigh-Plesset type equation for an average bubble evolution. Such an equation will include implicitly the drug, surface tension, and viscous forces, and the mass transfer due to the phase transition. The model will be applied to future studies of processes in the Muon Collider/Neutrino Factory target as well as hydrodynamic aspects of the cavitation induced erosion in the target for the Spallation Neutron Source.

Acknowledgments: The authors are grateful to James Glimm, Harold Kirk, Kirk McDonald, Xiaolin Li, Myoung-Nyoun Kim, and Adrian Fabich for fruitful discussions. Financial support has been provided by the USA Department of Energy, under contract number DE-AC02-98CH10886.

References

[1] Chandrasekhar, S.: *Hydrodynamic and Hydrodynamic stability*, Clarendon press, (Oxford, 1961).

[2] Cheng, B., Glimm, J., Sharp, D.H., Dynamical Evolution of the Rayleigh-Taylor and Richtmyer-Meshkov Mixing Fronts. Phys. Rev. E **66**, 1–7 (2002).

[3] Courant, R., Friedrichs, K.: *Supersonic Flows and Shock Waves*, Interscience, (New York, 1948).

[4] Dimonte, G., Nonlinear evolution of the Rayleigh-Taylor and Richtmyer-Meshkov instabilities. Phys. Plasmas **6**, 2009–2015 (1999).

[5] Dimonte, G., Remington, B., Richtmyer-Meshkov experiments on the Nova laser at high compression. Phys. Rev. Lett. **70** (1993) 1806–1809.

[6] Fabich, A., Lettry J., Experimental Observation of Proton-Induced Shocks and Magneto-Fluid-Dynamics in Liquid Metal, proceedings NuFact 01, NIM A, (2001).

[7] Fabich, A., High Power Proton Beam Shocks and Magnetohydrodynamics in a Mercury Jet Target for a Neutrino Factory, CERN-THESIS-2002-038, Vienna, November (2002).

[8] Glimm, J., Grove, J. W., Li, X.L., Shyue, K.L, Zhang, Q., Zeng, Y., Three dimensional front tracking. SIAM J. Sci. Comp. **19**, 703-727 (1998).

[9] Glimm J., Grove J., Li X.-L, and Tan D.C., Robust computational algorithms for dynamic interface tracking in three dimensions, SIAM J. Sci. Comp. **21**, 2240-2256, (2000).

[10] Glimm, J., Samulyak R., et al., Simulation of 3D fluid jets with application to the Muon Collider target design. Advances in Fluid Mechanics III. WIT Press, Southampton Boston, 191 - 200 (2000)

[11] Grove, J.W., Holmes, R., Sharp, D.H., Yang, Y., Zang, Q., Quantitative Theory of Richtmyer-Meshkov Instability. Phys. Rev. Lett. **71**, 3473–3476 (1993).

[12] Jackson, D. J.: *Classical Electrodynamics*, John Wiley & Sons, (New York, Toronto, Singapore, 1974).

[13] Johansen, H. and Colella, P., A Cartesian grid embedded boundary method for Poisson's equation on irregular domains, Journal of Comp. Phys. **147**, 60–85 (1998).

[14] Kane, J., Drake, R.P., Remington, B.A., An evaluation of the Richtmyer-Meshkov instability in supernova remnant formation. Astrophys. J. **511**, 335-340, (1999).

[15] Kirk, H., et al.: Target studies with BNL E951 at the AGS. Particles and Accelerators 2001, Chicago IL, June 18-22 (2001).

[16] Landau, L.D., Lifshitz, E.M.: *Electrodynamics of Continuous Media*, Addison - Wesley Publishing Co., (Reading Massachusetts 1960).

[17] Menikoff, R., Plohr, B., The Riemann problem for fluid flow of real materials. Rev. Mod. Phys. **61**, 75-130, (1989).

[18] Moreau, R.: *Magnetohydrodynamics*, Kluwer Academic Publishers, (Dordrecht - Boston - London, 1990).

[19] Mokhov, N.V., MARS Code Developments, Benchmarking and Applications, Fermilab-Conf-00-066 (2000).

[20] Ozaki, S., Palmer, R., Zisman, M., Gallardo, J. (editors): Feasibility Study- II of a Muon-Based Neutrino Source. BNL-52623 (2001).

[21] Samulyak, R., Numerical simulation of hydro- and magnetohydrodynamic processes in the Muon Collider target, Lecture Notes in Comp. Sci., Vol. 2331. Springer-Verlag, 391–400 (Berlin Heidelberg New York, 2002).

[22] Wallis, G.B., *One-dimensional Tho-phase Flow*, McGraw-Hill, (New York, 1969).

[23] van Wijngaarden, L., One-dimensional flow of liquids containing small gas bubbles, Ann. Rev. Fluid Mech. **4**, 369–396 (1972).

[24] Taleyarkhan, R.P., Moraga, F. and West C.D., Experimental Determination of Cavitation Thresholds in Liquid Water and Mercury , Proc. 2 nd Int. Meeting on Nuclear Applications of Accelerator Technology (AccApp 98), Gatlinburg, TN, Am. Nucl. Soc., Sept. 20-23 (1998).